Published in final edited form as:

Mol Pharm. 2017 May 01; 14(5): 1538–1547. doi:10.1021/acs.molpharmaceut.7b00050.

Development of surface-variable polymeric nanoparticles for drug delivery to tumors

Ning Han[1,2], **Liang Pang**[1,3], **Jun Xu**[1], **Hyesun Hyun**[1], **Jinho Park**[1,4], and **Yoon Yeo**[1,5,*]

[1]Department of Industrial and Physical Pharmacy, Purdue University, 575 Stadium Mall Drive, West Lafayette, IN 47907, USA

[2]Department of Pharmaceutics, School of Pharmacy, Shenyang Pharmaceutical University, 103 Wenhua Road, Shenyang, Liaoning 110016, PR China

[3]Department of Pharmaceutics, School of Pharmacy, Fudan University, 826 Zhangheng Road, Shanghai, 201203, PR China

[4]Lilly Research Laboratories, Lilly Corporate Center, Eli Lilly and Company, Indianapolis, IN 46285, USA

[5]Weldon School of Biomedical Engineering, Purdue University, 206 South Martin Jischke Drive, West Lafayette, IN 47907, USA

Abstract

To develop nanoparticle drug carriers that interact with cells specifically in the mildly acidic tumor microenvironment, we produced polymeric nanoparticles modified with amidated TAT peptide via a simple surface modification method. Two types of core poly(lactic-co-glycolic acid) nanoparticles (NL and NP) were prepared with a phospholipid shell as an optional feature and covered with polydopamine that enabled the conjugation of TAT peptide on the surface. Subsequent treatment with acid anhydrides such as cis-aconitic anhydride (CA) and succinic anhydride (SA) converted amines of lysine residues in TAT peptide to β-carboxylic amides, introducing carboxylic groups that undergo pH-dependent protonation and deprotonation. The nanoparticles modified with amidated TAT peptide (NLpT-CA and NPpT-CA) avoided interactions with LS174T colon cancer cells and J774A.1 macrophages at pH 7.4 but restored the ability to interact with LS174T cells at pH 6.5, delivering paclitaxel efficiently to the cells following a brief contact time. In LS174T tumor-bearing nude mice, NPpT-CA showed less accumulation in the lung than NPpT, reflecting the shielding effect of amidation, but tumor accumulation of NPpT and NPpT-CA was equally minimal. Comparison of particle stability and protein corona formation in media containing sera from different species suggests that NPpT-CA have been activated and opsonized in mouse blood to a greater extent than those in bovine serum-containing medium, thus losing the benefits of pH-sensitivity expected from in-vitro experiments.

*Corresponding author: Yoon Yeo, Ph.D. Phone: 765.496.9608, Fax: 765.494.6545, yyeo@purdue.edu.

Supporting Information Available: Supporting Figures are available free of charge via the Internet at http://pubs.acs.org.

Keywords

PLGA nanoparticles; TAT peptide; acid anhydrides; pH sensitive; drug delivery

1. Introduction

Chemotherapy plays an essential role in cancer treatment, but the lack of target specificity leads to severe side effects and suboptimal therapeutic efficacy. Various types of nanocarriers such as liposomes, polymeric micelles, polymeric or inorganic nanoparticles have been developed to achieve tumor-targeted drug delivery. The premise of nanoparticle-based chemotherapy is that nanoparticles have preferential access to tumors via the leaky vasculature,[1] and therefore bring anti-cancer drugs to tumors more selectively than free drugs. To achieve selective tumor accumulation via the leaky vasculature, the surface of nanoparticles is typically modified with hydrophilic polymers such as polyethylene glycol (PEG). However, the presence of PEG can interfere with the particle-cell interactions and the cellular uptake of the particles in the target tissues.[2, 3]

To overcome this challenge, we propose to decorate the nanoparticle surface with TAT peptide, which can help bring the nanoparticles into cells. TAT is a cell-penetrating peptide and has been conjugated to proteins, genes, and nanoparticles to facilitate their cellular uptake and/or intracellular trafficking.[4–9] TAT peptide establishes electrostatic interactions with negatively charged proteoglycans of the cell membrane via basic amino acids, activate permeabilization of the cell membrane through a receptor-independent pathway, and facilitate the endocytosis of the conjugated cargo.[10] For example, TAT was conjugated to mesoporous silica nanoparticles to facilitate their intra-nuclear localization and drug delivery to the nuclei.[11] This system allowed the drug to bypass P-gp drug efflux pump and overcome multidrug resistance of cancer cells and released the loaded drug (doxorubicin) directly in the nucleoplasm. TAT peptide has also been incorporated in micellar assemblies of amphiphilic peptides[12] or block-co-polymers[13] and helped them to deliver gene therapeutics into cells. Despite the benefits of TAT peptide, its interactions with cells are non-specific and remain a concern in the delivery of toxic chemotherapeutic agents.[8] Therefore, we intend to shield the peptide during circulation and deploy the peptide only at the tumor site. Tumor microenvironment is known to be different from normal tissues in the pH,[14, 15] oxygen content,[16] and enzyme level,[17] which may be exploited as a way of triggering tumor-specific activation of the nanoparticle surface. In particular, pH-sensitive triggering has gained significant interest, since most xenografts and human tumors are characterized by slightly acidic microenvironment with pH values around 6.5–7.2, which stems from excessive production of lactic acid by tumor cells and high rate of metabolism.[18]

Several studies report strategies to induce pH-triggered deshielding of TAT conjugated to nanoparticles and accomplish tumor-specific drug delivery. For example, a pH-sensitive block copolymer polysulfonamide- block-polyethyleneglycol (PSD-b-PEG), which is negatively charged at pH 7.4 and forms electrostatic complexes with the positively charged TAT, was used to shield the TAT on the micelle surface and prevent the TAT-micelles from interacting with normal cells.[19] In the acidity of tumors, PSD-b-PEG became neutral and

detached from TAT, deshielding TAT and allowing the TAT-micelles to enter tumor cells. In other study, TAT was conjugated to nanoparticles via poly(L-histidine), which was non-ionized at neutral pH and bound to the hydrophobic nanoparticle surface consisting of poly(L-lactic acid) and poly(L-histidine). Such interactions between poly(L-histidine) and the nanoparticle core pulled TAT close to the nanoparticle surface hiding it under the PEG corona. At mild acidic pH, both poly(L-histidine linker) and nanoparticle core were positively charged, their interactions lost, and TAT was allowed to pop out beyond the PEG shell and interact with cells.[20] Another study uses acid-cleavable hydrazone bond to link PEG to nanoparticle surface to shield and deshield TAT conjugated to liposomes according to the pH change.[21] These approaches demonstrated a proof of concept in cell and animal models; however, the complexity of these approaches and the need for new polymers or phospholipids limit the broad applicability to different types of nanoparticle systems.

In this study, we employ an easy and versatile method to conjugate TAT peptide on nanoparticles and shield the peptide in a pH-sensitive manner. Polymeric nanoparticles with different surface properties are decorated with TAT via polydopamine (pD) layer that mimics adhesive mussel foot proteins.[22, 23] TAT is then shielded by simple treatment with organic acid anhydrides, which preferentially react with primary amine groups of lysine residues in TAT to form β-carboxylic amide bonds.[24] We expect that the added carboxylates will neutralize TAT at pH 7.4 but allow the peptide to restore the cell-interactive properties upon protonation in slightly acidic tumor microenvironment and facilitate the cellular uptake of nanoparticles. Here, we screen different acid anhydrides and amidation conditions for optimal shielding and deshielding of two types of nanoparticles and demonstrate their pH-dependent cellular uptake and drug delivery profiles. We investigate how the pH-sensitivity of nanoparticles translates to their biodistribution in tumor-bearing mice and discuss the challenges and future directions.

2. Experimental section

2.1 Materials

Poly(lactic-co-glycolic) acid (PLGA LA:GA = 85:15, 30 kDa, ester end capped) and Rhodamine-labeled PLGA (LA:GA = 50:50, 30 kDa, Rhodamine B end caped) were purchased from Akina, Inc. (West Lafayette, IN). DPPC and DSPE-PEG_{2000} were obtained from Avanti polar lipids, Inc. (Alabaster, Alabama). Dopamine-HCl was purchased from Alfa Aesar (Ward Hill, MA). Paclitaxel (PTX) was a gift from Samyang Genex Corp (Seoul, Korea). 3-(4,5-Dimethylthiazol-2-yl)-2,5-diphenyl tetrazolium bromide (MTT) and Hoechst 33342 were purchased from Invitrogen (Eugene, OR). TAT peptide (CKYGRRRQRRKKRG) was synthesized by GenScript USA (Piscataway, NJ). All other chemicals were obtained from Sigma-Aldrich (St. Louis, MO) unless otherwise specified. Deionized (DI) water was obtained from an ultrafiltration system (Milli-Q, Millipore). Human serum and Balb/C mouse serum were obtained from Innovative research (Novi, MI).

2.2 Preparation of nanoparticles (Fig. 1)

2.2.1 Core nanoparticles—Two types of core nanoparticles were prepared. First, PLGA nanoparticles were prepared by the single emulsion method with polyvinyl alcohol (PVA) as

an emulsifier and referred to as NP. Twenty milligrams of PLGA (LA:GA = 85:15, MW 30k) was dissolved in 1 mL of dichloromethane (DCM) and added to 4 mL of 4% PVA solution, followed by probe sonication (Sonics Vibracell, Newtown, CT) for 2 min with a 4s-on and 2s-off pulse setting at an amplitude of 40W. Lipid-shelled nanoparticles (referred to as NL) were prepared by dissolving 20 mg PLGA, 2 mg DPPC and 2 mg DSPE-PEG_{2000} in 0.6 mL DCM, mixing with 8 mL DI water, and sonicating for 2 min with a 4s-on and 2s-off pulse setting. For both nanoparticles, the formed emulsion was evaporated by a rotary evaporator to remove the DCM and solidify the particles. The particles were then collected via centrifugation at 33,900 ×g at 4 °C and washed with DI water two times. In preparing fluorescently labeled particles for flow cytometry or confocal microscopy, 12 mg of PLGA was replaced with Rhodamine-labeled PLGA. When paclitaxel (PTX) or DiR were loaded, they were dissolved in the organic phase together with PLGA at a theoretical PTX content of 5 wt% and DiR content of 0.5 wt%, respectively.

2.2.2 TAT conjugation on nanoparticle surface via polydopamine—To create the pD-coated particles (NPp and NLp), 2 mg of NP and NL were re-dispersed in 1 mL of 10 mM Tris buffer (pH 8.5) containing 0.5 mg/mL dopamine HCl and stirred for 2h at room temperature (RT). The obtained NPp and NLp were washed with DI water two times to remove excess dopamine. For TAT-conjugation (NPpT and NLpT), 2 mg of NPp or NLp were re-suspended in 0.6 mL of Tris buffer containing 3 mg/mL of TAT peptide and incubated for 2h (NPp) or 30 min (NLp) at RT with constant rotation. The particles was collected by centrifugation and washed with Tris buffer and 10 mM phosphate buffer (pH 7.4) two times to remove excess TAT.

2.2.3 TAT shielding via acid anhydrides—For shielding TAT peptide on the particle surface, the NPpT and NLpT particles were dispersed in sodium carbonate buffer (0.1 M, pH 9), to which fresh acid anhydrides (10 mM for NPpT and 15 mM for NLpT) were added and incubated for 0.5–1h. After anhydride treatment, the particles were centrifuged and washed with phosphate buffer (pH 7.4) twice. The anhydride-treated particles were called NPpT-CA (cis-aconitic anhydride-treated NPpT), NPpT-SA (succinic anhydride-treated NPpT), and NPpT-DA (2,3-dimethylmaleic anhydride-treated NPpT), NLpT-CA (cis-aconitic anhydride-treated NLpT), NLpT-SA (succinic anhydride-treated NLpT), and NLpT-DA (2,3-dimethylmaleic anhydride-treated NLpT), according to the type of particles and acid anhydride.

2.3 Particle characterization

Particle size was determined with particles dispersed in DI water, and zeta potential were measured with particles in phosphate buffer (5 mM) with pH 7.4 or 6.5, using a Malvern Zetasizer Nano ZS90 (Worcestershire, UK). The morphology of particles was observed by transmission electron microscopy (TEM) using Tecnai F20 (FEI, Hillsboro, OR). Samples were negatively stained by 2% uranyl acetate prior to imaging.

2.4 Quantification of TAT conjugation and amidation

TAT peptides present on the surface of nanoparticles (NPpT, NLpT, NPpT-CA, and NLpT-CA) were quantified by the ninhydrin assay, based on the reaction between ninhydrin and

primary amines that produces a chromophore called Ruhemann's purple.[26] A known mass (1.6 – 1.7 mg) of particles were dispersed in 0.5 mL of water and mixed with 0.5 mL of freshly prepared ninhydrin reagent. The mixture was incubated at 100 °C for 20 min and cooled down in ice for 2 min. The sample was mixed with 0.5 mL of ethanol and centrifuged for 20 min at 16,000 ×g. The absorbance of supernatant was detected at 570 nm. NPp or NLp were used as background controls to account for the interference of pD. The TAT contents in particles were calculated based on the absorbance difference between NPp (or NLp) and TAT-modified NPp (or TAT-modified NLp) and a calibration curve prepared with standard TAT peptide solutions. For easy comparison, the TAT content was expressed as the number of TAT peptides per 100 nm^2 of particle surface. The extent of amidation was calculated based on the reduction of the absorbance, under an assumption that only lysine residues can react with ninhydrin to generate Ruhemann's purple.

2.5 In vitro drug release

Particles equivalent to 3.5 μg PTX were dispersed in 1 mL of phosphate buffered saline containing 0.2% Tween 80 (PBST). The samples were kept at 37°C with consistent rotation. At predetermined time points, samples were centrifuged at 33,900 ×g, and 0.8 mL of supernatant was withdrawn and replaced with fresh PBST. The particles were redispersed by sonication and returned to the rotation at 37 °C. The sampled supernatant was filtered through a 0.22 μm syringe filter to measure the released PTX by HPLC. The amount of released PTX was analyzed using an Agilent 1100 HPLC system (Palo Alto, CA) equipped with Ascentis C18 column (25 cm × 4.6 mm, particle size 5 mm). The mobile phase was composed of water and acetonitrile (50:50) running at a flow rate of 1 mL/min. PTX was detected by a UV detector at wavelength of 227 nm.

2.6 Cell culture

LS174T human colon cancer cells and J774A.1 murine macrophages (ATCC, Manassas, VA) were respectively grown in MEM and DMEM medium containing 10% fetal bovine serum (FBS), 100 U/mL of penicillin and 100 mg/mL of streptomycin at 37 °C and 5% CO_2. All cell experiments were performed in complete media.

2.7 In vitro cell-nanoparticle interaction

2.7.1 Flow cytometry—LS174T cells or J774A.1 macrophages were seeded in 24-well plates and incubated overnight. The culture medium was replaced with 0.3 mg/mL of Rhodamine-labeled particles in culture medium with different pH values (pH 7.5 and pH 6.5). After 2h incubation, the particles were removed, and cells were washed with fresh medium with corresponding pHs twice. Finally, the cells were trypsinized and collected, the fluorescence intensity of the cells was quantified using an Accuri C6 flow cytometer (BD Biosciences, San Jose, CA) equipped with an FL-2 detector ($\lambda_{ex}/\lambda_{em}$ = 585/625 nm).

2.7.2 Confocal microscopy—To visualize the cellular uptake of particles at pH 7.4 and 6.5, LS174T cells were seeded in a 35 mm glass-bottomed Petri dish (MatTek Corp., Ashland, MA). After treatment with the Rhodamine-labeled particles for 2h, the cells were washed with fresh medium and PBS and fixed with 4% paraformaldehyde. After staining the

nuclei with Hoechst 33342 (2 μg/mL) for 15 min, images were taken with a Nikon-A1R confocal microscope (Nikon America Inc., Melville, NY).

2.8 Cell viability

LS174T cells were seeded in 96 well plates with a density of 10,000 cells per well and incubated overnight. PTX-loaded particles were added to each well to make the final PTX concentration of 1-10000 nM. After incubation with cells for 2h at pH 7.4 and 6.5, particles were removed and replaced with 100 μL of fresh culture medium. The cells were allowed to grow for 24h, and 15 μL of MTT solution (5mg/mL) was subsequently added to each well and incubated at 37 °C for 4h. Finally, 150 μL of stop/solubilization solution was added to each well. The plate was agitated at 37 °C overnight and the absorbance was measured at 562 nm with a SpectraMax M3 microplate reader (Molecular Devices, Sunnyvale, CA).

2.9 Nanoparticle distribution in tumor-bearing mice

All animal procedures were approved by Purdue Animal Care and Use Committee, in conformity with the NIH guidelines for the care and use of laboratory animals. A xenograft model was established by subcutaneous injection of 5×10^6 LS174T cells on the upper flank of right thigh of 7–8 week old female athymic nude mice. When the average tumor volume reached 400–600 mm^3, animals were injected with different particles containing DiR through tail vein. Each animal received 0.4 mg of particles (equivalent to 0.5 μg DiR) suspended in 0.2 mL of PBS (pH 7.4). NIR fluorescence images were taken under 3% isoflurane anesthesia at different time intervals using SPECTRAL Ami Imaging Systems (Spectral Instruments Imaging, LLC, Tucson, AZ) with an excitation and emission wavelength of 745 nm and 790 nm, respectively.

2.10 Particle stability in serum

To compare the stability of modified surface in sera of different species, 2 mg of Rhodamine-labeled NPpT-CA was incubated in 50% FBS, 50% human serum (HS) or 50% mouse serum (MS) at 37 °C for 2h. Afterwards, the particles were collected by centrifugation and washed once with 0.5 mL of PBS. The particles were diluted with complete culture medium to 0.3 mg/mL and incubated with J774A.1 macrophages seeded in a 24 well plate for 2h. After the removal of particles, the cells were collected and re-dispersed in 0.5 mL of serum-free medium. The extent of macrophage uptake of particles was quantified by flow cytometry.

2.11 Protein absorption to particle surfaces

To compare protein binding to particles after incubation in sera of different species, 2 mg NPpT-CA were incubated in 2 mL of 50% FBS, 50% HS and 50% MS for 2h. The particles were collected by centrifugation and washed with PBS (pH 7.4) once. Samples were prepared by mixing 75 μL of 5 mg/mL particle suspension with 25 μL of Laemmli sample buffer and heating at 95 °C for 5 min. The samples were analyzed with sodium dodecyl sulfate (SDS)-polyacrylamide (PAGE) gel electrophoresis and stained with Coomassie Blue.

2.12 Statistical analysis

All statistical analysis was performed with GraphPad Prism 6. All in vitro data were analyzed with one-way or two-way ANOVA test to determine the difference of means among groups, followed by Dunnett's or Sidak's multiple comparisons test. A value of $p < 0.05$ was considered statistically significant.

3. Results and discussion

3.1 Characterization of NL and NP

As seen in the TEM image (Fig. 2), NL and NP were spherical particles with an average diameter of 120 nm and 100 nm, respectively. Polydispersity index (PDI) of these particles was close to 0.1, which indicates reasonably homogeneous particle size distribution (Table 1). The particle sizes of NL and NP measured by dynamic light scattering were substantially larger than those estimated by TEM. This difference may not be explained by the hydration layer surrounding the particles dispersed in water, which is typically no more than a few nanometers. The large particle size measured in DLS rather reflects the extent of nanoparticle aggregation, which occurs with repeated washing and centrifugation. NL showed negative charges at both pH 7.4 and 6.5 due to the phosphate group located at the outer region of the lipid head,[27] whereas NP with bare surface of ester-capped PLGA and some residual PVA were close to neutral.

3.2 Characterization of surface-modified NL and NP

After dopamine treatment, both particles showed dark gray color, indicating the presence of polymerized dopamine layer, which was identified as a wrinkled layer on the particle surface in TEM images. There were no additional differences in TEM images with subsequent conjugation of TAT and anhydride treatment, consistent with our previous observation of other ligand conjugation.[30] After pD coating, the zeta potential of NP, which was initially near neutral, became more negative due to the catechol hydroxyl groups of the surface pD (Fig. 3). On the other hand, the zeta potential of NL increased slightly after pD coating, indicating partial coverage of the negatively charged phosphate groups of the lipid by less negatively charged pD layer.

The amount of TAT peptide conjugated to the nanoparticle surface was determined by the ninhydrin assay (Supporting Fig. 1). The average numbers of TAT peptides present on NPpT and NLpT were 9.0 ± 2.8 per 100 nm^2 (0.85 ± 0.27 wt%) and 22.7 ± 3.5 per 100 nm^2 (1.54 ± 0.23 wt%), respectively. The relatively high TAT conjugation to NLp may be due to the greater negative charge of NLp, which can attract TAT peptide via electrostatic interactions as well as the reactivity of pD. The numbers of TAT peptides present on NPpT-CA and NLpT-CA were calculated to be 4.2 ± 2.7 per 100 nm^2 (0.40 ± 0.26 wt%) and 12.4 ± 1.5 per 100 nm^2 (0.84 ± 0.10 wt%), which correspond to 46% of NPpT and 55% of NLpT, respectively. Assuming that only lysine residues produce the Ruhemann's purple in the ninhydrin reaction (i.e., absorbance at 570 nm due to arginine residues is negligible),[26] we estimate that 54% of TAT on NPpT and 45% of TAT on NLpT were amidated by CA treatment. TAT conjugation to NLp was also confirmed by H-NMR. Both NLpT and NLpT-CA, but not NLp, showed TAT signals at 3.15 and 4.12 ppm. CA amidation could not be

identified due to the interference of PLGA, pD, and lipids. We suspect the signal might be overlapping with others at ~3.5 ppm (Supporting Fig. 2).

Surface charges of TAT and anhydride-treated nanoparticles were consistent with the modification of the nanoparticle surface (Fig. 3). After TAT modification, surface charges of particles increased from negative values (NLp and NPp) to near neutral values (NLpT and NPpT), irrespective of the pH, due to the lysine and arginine residues of TAT. On the other hand, NLpT and NPpT treated with anhydrides (NLpT-DA, NLpT-SA, NLpT-CA, and NPpT-CA) showed much more negative charges than NLpT and NPpT at pH 7.4. At pH 6.5, these particles showed less negative charges. The particle size measured by DLS increased after each surface modification step (Table 1). Given no visible changes in the particle morphology and the increase of PDI, the particle size increase is attributed to the repeated washing and aggregation. NL series showed greater size increase than NP series, most likely due to the lack of residual emulsifier (PVA). NLpT with neutral charge was particularly prone to aggregation. NPpT was relatively resistant to aggregation despite the neutral charge, likely due to the residual PVA.

3.3 Mechanism of pH-sensitivity of anhydride-treated particles

In order to understand how anhydride-treated particles showed pH-sensitive charge profiles, the zeta potential of the particles was measured in alternating pHs. According to the literature, β-carboxylic amide is cleaved in mildly acidic condition to regenerate corresponding amine.[24] Therefore, we expected that the amidated TAT would remain shielded at neutral pH but convert to the original TAT after the incubation in acidic buffer due to the cleavage of β-carboxylic amide bond. To test this, NLpT-anhydrides were incubated in buffers with pH 6.5 and pH 5 for 2h, washed and re-dispersed in 10 mM phosphate buffer (pH 7.4). After this treatment, NLpT-DA showed the same surface charge as NLpT as expected (Supporting Fig. 3). However, NLpT-CA and NLpT-SA treated in the same way did not display the surface charge of NLpT but showed the same value as fresh NLpT-CA and NLpT-SA. This result indicates that β-carboxylic amide bonds in the amidated TAT of NLpT-CA and NLpT-SA were not hydrolyzed in acidic pH in 2h. Instead, the carboxylic groups remained in the peptide and underwent pH-dependent deprotonation. This difference is largely due to the structure of anhydride used to modify TAT. In general, double bond or alkyl substituents to the α,β-position of anhydride give rise to more sensitive β-carboxylic amide.[31] DA has a double bond and two methyl groups at α and β positions, thus generating hydrolyzable β-carboxylic amide bond quickly, whereas the amide from SA is relatively stable even at very low pH values.[31] With a double bond and single alkyl substitution, CA appears to produce an amide bond with intermediate stability.

3.4 In vitro cellular uptake

LS174T colon cancer cells incubated with NL, NP, NLp, and NPp showed low fluorescence intensity corresponding to little cellular interaction, irrespective of the pH (Fig. 4). After TAT modification, the cell-particle interaction significantly increased due to the cell penetrating capability of TAT. DA, SA, and CA showed different efficiency of shielding and deshielding of TAT, consistent with the stability of β-carboxylic amides discussed in the previous section. DA proved to be the least effective in shielding TAT at pH 7.4, showing

little decrease of cellular interaction (NLpT-DA, NPpT-DA). Both SA and CA-treated particles showed significantly reduced interaction with LS174T cells at pH 7.4, indicating successful shielding of TAT. At pH 6.5, both SA and CA-treated particles showed increased cellular uptake, which suggests that, in the absence of the cleavage of β-carboxylic amide bonds, the protonation of the added carboxylic groups was sufficient to restore the peptide's ability to interact with cells. Between SA and CA, the latter showed more consistent shielding and deshielding effects in both types of particles, likely due to the additional carboxylic group; therefore, CA was used for the rest of the study. In addition to the type of anhydride, the treatment conditions also played a role in determining efficient shielding and deshielding of TAT. NLpT-CA and NPpT-CA were produced varying the amount of added CA (Supporting Fig. 4). During the amidation reaction, CA also undergoes hydrolysis. Efficient amidation requires supplementation of fresh CA. Insufficient or excessive CA results in incomplete shielding of TAT or inefficient restoration of the peptide's ability to interact with cells, respectively.

Confocal images showed a consistent trend as flow cytometry (Fig. 5). LS174T cells treated with NL and NP showed little fluorescence signal of the particles at either pH, indicating minimal cell-particle interactions. With TAT-modified particles (NLpT and NPpT), strong red fluorescence signals were seen at the periphery of cell clusters irrespective of the pH conditions. For the cells treated with NLpT-CA and NPpT-CA, there were virtually no fluorescence signals at pH 7.4, indicating the lack of interactions between the particles and the cells. At pH 6.5, fluorescence signals at the periphery of the cell clusters were clearly seen, similar to those treated with NLpT and NPpT. This result is consistent with flow cytometry data (Fig. 4) and confirms that CA-treated TAT was effectively shielded at neutral pH and restored the ability to interact with cells at mildly acidic pH. NLpT-SA showed a similar trend as NLpT-CA (Supporting Fig. 5). The flow cytometry and confocal microscopy results, taken together, suggest that NLpT-CA or NPpT-CA shall preferentially interact with tumor cells in acidic microenvironment, sparing cells in normal pH. The nature of cell-nanoparticle interaction is likely to be electrostatic interaction, given that there was a strong correlation ($r^2 = 0.9006$) between the surface charge of particles and fluorescence intensity of LS174T cells representing the particles associated with the cells (Supporting Fig. 6).

Since the prerequisite of nanoparticle delivery to tumors is to avoid the phagocytic clearance of nanoparticles in circulation, we tested whether the shielding effect extended to the prevention of macrophage uptake of the nanoparticles (Supporting Fig. 7). Consistent with the interactions with LS174T cells, NP and NPp showed little interaction with macrophages, whereas macrophages treated with NPpT had much greater fluorescence intensity. With the CA treatment, NPpT-CA showed substantially reduced the interactions with macrophage as expected.

3.5 In vitro drug release

The particles slowly released PTX in PBST over 48h (Supporting Fig. 8). NP showed slightly higher burst release than NL in the initial 10h. However, after surface modification with TAT and anhydride, NPpT-CA showed lower initial burst release. NL and NLpT-CA showed similar release kinetics irrespective of TAT/anhydride modification. This result

suggests that NP had surface-bound PTX, which was washed out during the subsequent surface modification to NPpT-CA. On the other hand, the lipid layer of NL served as a protective coating to prevent the loss of PTX during the surface modification.

3.6 Cytotoxicity of PTX loaded particles

To test whether the pH-sensitive cell-nanoparticle interaction translates to pH dependent PTX delivery and cell killing, PTX-loaded particles were given to LS174T cells at pH 7.4 or 6.5 and incubated for 2h. This time frame was chosen because 2h is sufficient for establishing interactions with cells (Figs. 4 and 5) and PTX release by 2h was <30% of total dose (Supporting Fig. 8). After 2h incubation, the cells were removed of the particles and allowed to grow for another 24h prior to the viability measurement. As shown in Fig. 6, all particles showed dose-dependent cytotoxic effects. Notably, PTX-loaded NLpT-CA and PTX-loaded NPpT-CA showed greater cytotoxicity at pH 6.5 than at pH 7.4. PTX-loaded NL or PTX-loaded NP (bare particles) showed similar level of toxicity to those of NLpT-CA or NPpT-CA counterparts at pH 7.4, irrespective of the pH. This result indicates that NLpT-CA and NPpT-CA were able to establish better cell-particle interactions in acidic environment during the 2h incubation than those at pH 7.4 or bare particles in either condition, consistent with flow cytometry and confocal microscopy results.

3.7 Nanoparticle distribution in tumor-bearing mice

The in vitro results collectively suggest that NL(P)pT-CA will be retained in LS174T tumors, which are mildly acidic, better than NL(P)pT, due to the pH-sensitive interactions and ‘dis’interactions. To observe particle distribution via optical whole body imaging, the particles were loaded with DiR, a hydrophobic near infrared (NIR) fluorescence dye. Unlike a commonly used NIR dye indocynine green (ICG), which is hydrophilic and has high affinity for serum proteins,[32] DiR is stably retained in the PLGA particles in medium containing 50% FBS, a condition mimicking the protein content in blood (Supporting Fig. 9), and thus serves as a reasonable tracer of nanoparticles in circulation. We confirmed that DiR-loaded NP mainly accumulated in the liver and spleen, common destinations of intravenously administered nanoparticles. In contrast, ICG released rapidly from ICG-loaded NP in 50% FBS. In mice receiving ICG-loaded NP, the fluorescence signal appeared in the gastrointestinal tract, following the typical distribution of free ICG.[33] Therefore, we chose DiR as a fluorescence label of particles for in vivo imaging. We compared NPpT and NPpT-CA to evaluate the effect of surface modification on tumor accumulation of the particles, because they showed consistently smaller particle sizes than NL counterparts (Table 1) and the size difference – another significant factor that can affect biodistribution – was much smaller (177.0 nm vs. 179.5 nm) than that of NLpT and NLpT-CA (411.3 nm vs. 270.3 nm).

NIR fluorescence images show that both NPpT and NPpT-CA appeared in the liver and spleen in 30 min after intravenous injection. The fluorescence signal intensity gradually decreased with time, showing no detectable signals at tumor sites in both cases (Fig. 7a, Supporting Fig. 10). The ex vivo images obtained at 48h post injection (Fig. 7b) verified the intense fluorescence signals in the liver and spleen. No signals were seen in tumors. A notable difference between the two groups is that NPpT showed signals in the lung but NPpT-CA did not. We confirmed that the particle sizes of the two types of particles

remained the same in PBS prior to the injection; therefore, the lung signal difference is attributable to the surface properties. While NPpT were non-specifically captured in the lung capillary due to the cationic amino acid residues of TAT, NPpT-CA with the shielded TAT avoided such interactions.

3.8 Potential factors to interfere with in-vitro-in-vivo correlation

LS174T xenograft is a well vascularized tumor and known to develop leaky vasculature.[34, 35] Therefore, we found it curious that the two types of particles did not show differential signals in tumors as they did in the lung. We first speculated that NPpT-CA was not sufficiently stable in circulation and prematurely activated. Although all the in vitro cell studies were performed in serum containing medium and indicated favorable cell-particle interaction profiles, the concentration (10%) and the origin (bovine) are different than those of mouse blood and may not necessarily reflect risk factors that would have affected the stability of NPpT-CA. To test if NPpT-CA has different sensitivity in sera from different species and/or different concentrations, we treated the Rhodamine-labeled NPpT-CA in 50% FBS, 50% human serum (HS), and 50% mouse serum (MS) for 2h prior to the incubation with macrophages. The NPpT-CA pre-treated with 50% FBS did not show any difference from PBS-treated NPpT-CA in the extent of macrophage interactions (Supporting Fig. 11). On the other hand, those pre-treated with 50% HS and MS showed increased macrophage interaction compared to PBS-treated NPpT-CA. This result indicates that NPpT-CA has greater sensitivity to MS but not necessarily to the high serum concentration. Secondly, we wondered if NPpT-CA developed protein corona prone to phagocytic clearance. Circulating nanoparticles, even with a protective surface layer, obtain protein corona that can interfere with intended interactions between the particles and target cells.[36, 37] Although NPpT-CA avoided macrophage interactions in the in-vitro test performed in FBS-containing medium, it is possible that they may contract with opsonins to a greater extent in sera from other species than in FBS. To test this, we analyzed proteins bound to NPpT-CA after incubation in 50% FBS, HS, or MS by gel electrophoresis (Supporting Fig.12). Compared to the NPpT-CA incubated in FBS, which had a dominant albumin band, those incubated in HS and MS showed more complex corona profiles in addition to albumin, reflecting the composition of each serum.

These results suggest that NPpT-CA have undergone premature activation and opsonization while circulating in mice, which were not properly predicted in the in-vitro studies performed in FBS-containing medium. On the other hand, given that NPpT-CA did show different lung distribution than NPpT despite the unfavorable changes, we envision that additional barrier may prevent tumor distribution of the particles. For example, the interstitial fluid pressure of tumors has long been recognized as a substantial obstacle to the transcapillary and intratumoral transport of drugs and nanoparticles.[38]

At present there is no ideal in-vitro method that can predict in-vivo performance of nanoparticle systems. Our study underscores the need for implementing routine in-vitro methods to better predict their in-vivo outcomes. First, it will be worthwhile to test the stability of nanoparticles in medium containing serum of matching species in a physiologically relevant concentration as performed in this study. In addition, an established

in-vitro protocol may be followed to examine protein corona formation and identify the particles that can maintain the chemical identity in concentrated serum.[39] In addition, in-silico model of cancer patients will make an invaluable tool to predict the biodistribution of nanoparticles. The kinetics and extents of drug release, protein corona formation, and particle size change in blood constitute critical information in in-silico modeling of drug and nanoparticle distribution and, thus, need to be defined as part of routine in-vitro characterization practices.

4. Conclusions

Dopamine polymerization method allowed easy and versatile surface modification of nanoparticles with TAT peptide. Additional anhydride treatment of the surface-bound TAT allowed pH-sensitive cell-nanoparticle interactions by converting lysine residue amines in TAT to β-carboxylic amides. At pH 7.4, the TAT-conjugated, cis-aconitic anhydride-treated particles (NLpT-CA and NPpT-CA) had minimal interactions with LS174T colon cancer cells and J774A.1 macrophages. At pH 6.5 representing weakly acidic tumor microenvironment, the CA-treated TAT layer underwent protonation and restored the ability to interact with cells, delivering PTX efficiently to the cells following a short contact time. Consistent with the shielding effect of CA treatment seen in vitro, NPpT-CA showed less accumulation in the lung than NPpT in LS174T tumor-bearing animals; however, tumor accumulation of NPpT and NPpT-CA was equally minimal. Potential reasons for this discrepancy include premature activation and opsonization of NPpT-CA circulating in mouse blood, which were not predicted in the in vitro experiments performed in bovine serum-containing medium.

Supplementary Material

Refer to Web version on PubMed Central for supplementary material.

Acknowledgments

This work was supported by NIH R01 EB017791 and the fellowship support from the China Scholarship Council Fellowship to N.H. and L.P., the Lilly Endowment Gift Graduate Research Award to J.X. and H.H., and the Lilly Innovation Fellowship Award to J.P. We thank the Bindley Bioscience Imaging Facility for technical support of the animal imaging experiments. The authors also thank Yihua Pei and Fanfei Meng for their kind discussion and suggestions.

References

1. Torchilin V. Tumor Delivery of Macromolecular Drugs Based on the EPR Effect. Adv Drug Deliv Rev. 2011; 63:131–135. [PubMed: 20304019]
2. Hatakeyama H, Akita H, Harashima H. A Multifunctional Envelope Type Nano Device (MEND) for Gene Delivery to Tumours Based on the EPR Effect: A Strategy for Overcoming the PEG Dilemma. Adv Drug Deliv Rev. 2011; 63:152–160. [PubMed: 20840859]
3. Hama S, Itakura S, Nakai M, Nakayama K, Morimoto S, Suzuki S, Kogure K. Overcoming the Polyethylene Glycol Dilemma via Pathological Environment-Sensitive Change of the Surface Property of Nanoparticles for Cellular Entry. J Control Release. 2015; 206:67–74. [PubMed: 25770398]

4. Nischan N, Herce HD, Natale F, Bohlke N, Budisa N, Cardoso MC, Hackenberger CP. Covalent Attachment of Cyclic TAT Peptides to GFP Results in Protein Delivery into Live Cells with Immediate Bioavailability. Angew Chem Int Ed. 2015; 54:1950–1953.
5. Astriab-Fisher A, Sergueev DS, Fisher M, Ramsay Shaw B, Juliano RL. Antisense Inhibition of P-Glycoprotein Expression Using Peptide–Oligonucleotide Conjugates. Biochem Pharmacol. 2000; 60:83–90. [PubMed: 10807948]
6. Pan L, He Q, Liu J, Chen Y, Ma M, Zhang L, Shi J. Nuclear-Targeted Drug Delivery of TAT Peptide-Conjugated Monodisperse Mesoporous Silica Nanoparticles. J Am Chem Soc. 2012; 134:5722–5725. [PubMed: 22420312]
7. Wang F, Wang Y, Zhang X, Zhang W, Guo S, Jin F. Recent Progress of Cell-Penetrating Peptides as New Carriers for Intracellular Cargo Delivery. J Control Release. 2014; 174:126–136. [PubMed: 24291335]
8. Huang Y, Jiang Y, Wang H, Wang J, Shin MC, Byun Y, He H, Liang Y, Yang VC. Curb Challenges of the “Trojan Horse” Approach: Smart Strategies in Achieving Effective yet Safe Cell-Penetrating Peptide-Based Drug Delivery. Adv Drug Deliv Rev. 2013; 65:1299–1315. [PubMed: 23369828]
9. Li Z, Dong K, Huang S, Ju E, Liu Z, Yin M, Ren J, Qu X. A Smart Nanoassembly for Multistage Targeted Drug Delivery and Magnetic Resonance Imaging. Adv Funct Mater. 2014; 24:3612–3620.
10. Rizzuti M, Nizzardo M, Zanetta C, Ramirez A, Corti S. Therapeutic Applications of the Cell-Penetrating HIV-1 Tat Peptide. Drug Discov Today. 2015; 20:76–85. [PubMed: 25277319]
11. Pan L, Liu J, He Q, Wang L, Shi J. Overcoming Multidrug Resistance of Cancer Cells by Direct Intranuclear Drug Delivery Using TAT-Conjugated Mesoporous Silica Nanoparticles. Biomaterials. 2013; 34:2719–2730. [PubMed: 23337327]
12. Han K, Chen S, Chen WH, Lei Q, Liu Y, Zhuo RX, Zhang XZ. Synergistic Gene and Drug Tumor Therapy Using a Chimeric Peptide. Biomaterials. 2013; 34:4680–4689. [PubMed: 23537665]
13. Kanazawa T, Akiyama F, Kakizaki S, Takashima Y, Seta Y. Delivery of siRNA to the Brain Using a Combination of Nose-to-Brain Delivery and Cell-Penetrating Peptide-Modified Nano-Micelles. Biomaterials. 2013; 34:9220–9226. [PubMed: 23992922]
14. Volk T, Jaihde E, Fortmeyer HP, Glisenkamp KH, Rajewsky MF. pH in Human Tumour Xenografts: Effect of Intravenous Administration of Glucose. Br J Cancer. 1993; 68:492–500. [PubMed: 8353039]
15. Engin K, Leeper DB, Cater JR, Thistlethwaite AJ, Tupchong L, McFarlane JD. Extracellular pH Distribution in Human Tumors. Int J Hyperthermia. 1995; 11:211–216. [PubMed: 7790735]
16. Harris AL. Hypoxia–a Key Regulatory Factor in Tumour Growth. Nat Rev Cancer. 2002; 2:38–47. [PubMed: 11902584]
17. Egeblad M, Werb Z. New Functions for the Matrix Metalloproteinases in Cancer Progression. Nat Rev Cancer. 2002; 2:161–174. [PubMed: 11990853]
18. Lee ES, Gao Z, Bae YH. Recent Progress in Tumor pH Targeting Nanotechnology. J Control Release. 2008; 132:164–170. [PubMed: 18571265]
19. Sethuraman VA, Bae YH. Tat Peptide-Based Micelle System for Potential Active Targeting of Anti-Cancer Agents to Acidic Solid Tumors. J Control Release. 2007; 118:216–224. [PubMed: 17239466]
20. Lee ES, Gao Z, Kim D, Park K, Kwon IC, Bae YH. Super Ph-Sensitive Multifunctional Polymeric Micelle for Tumor Ph(E) Specific Tat Exposure and Multidrug Resistance. J Control Release. 2008; 129:228–236. [PubMed: 18539355]
21. Koren E, Apte A, Jani A, Torchilin VP. Multifunctional PEGylated 2C5-Immunoliposomes Containing pH-Sensitive Bonds and TAT Peptide for Enhanced Tumor Cell Internalization and Cytotoxicity. J Control Release. 2012; 160:264–273. [PubMed: 22182771]
22. Lee H, Dellatore SM, Miller WM, Messersmith PB. Mussel-Inspired Surface Chemistry for Multifunctional Coatings. Science. 2007; 318:426–430. [PubMed: 17947576]
23. Lee H, Rho J, Messersmith PB. Facile Conjugation of Biomolecules onto Surfaces via Mussel Adhesive Protein Inspired Coatings. Adv Mater. 2009; 21:431–434. [PubMed: 19802352]
24. Jin E, Zhang B, Sun X, Zhou Z, Ma X, Sun Q, Tang J, Shen Y, Van Kirk E, Murdoch WJ, Radosz M. Acid-Active Cell-Penetrating Peptides for in Vivo Tumor-Targeted Drug Delivery. J Am Chem Soc. 2013; 135:933–940. [PubMed: 23253016]

25. Liebscher J, Mrowczynski R, Scheidt HA, Filip C, Hadade ND, Turcu R, Bende A, Beck S. Structure of Polydopamine: A Never-Ending Story? Langmuir. 2013; 29:10539–10548. [PubMed: 23875692]
26. Friedman M. Applications of the Ninhydrin Reaction for Analysis of Amino Acids, Peptides, and Proteins to Agricultural and Biomedical Sciences. J Agric Food Chem. 2004; 52:385–406. [PubMed: 14759124]
27. Makino K, Yamada T, Kimura M, Oka T, Ohshima H, Kondo T. Temperature- and Ionic Strength-Induced Conformational Changes in the Lipid Head Group Region of Liposomes as Suggested by Zeta Potential Data. Biophys Chem. 1991; 41:175–183. [PubMed: 1773010]
28. Dynamic Light Scattering – Common Terms Defined. Malvern Instruments Worldwide; Malvern, UK: 2014. MRK1764-01
29. International Organization for Standardization. ISO 22412:2008 (en) Particle size analysis – Dynamic light scattering (DLS). https://www.iso.org/obp/ui/#iso:std:iso:22412:ed-1:v1:en (accessed: December 10, 2016)
30. Park J, Brust TF, Lee HJ, Lee SC, Watts VJ, Yeo Y. Polydopamine-Based Simple and Versatile Surface Modification of Polymeric Nano Drug Carriers. ACS Nano. 2014; 8:3347–3356. [PubMed: 24628245]
31. Zhang, B., Wang, K., Si, J., Sui, M., Shen, Y. Charge-Reversal Polymers for Biodelivery. In: Gu, Z., editor. Bioinspired and Biomimetic Polymer Systems for Drug and Gene Delivery. Wiley-VCH Verlag GmbH & Co. KGaA; 2014. p. 223-242.
32. Muckle TJ. Plasma Proteins Binding of Indocyanine Green. Biochemical Medcine. 1976; 15:17–21.
33. Bahmani B, Lytle CY, Walker AM, Gupta S, Vullev VI, Anvari B. Effects of Nanoencapsulation and PEGylation on Biodistribution of Indocyanine Green in Healthy Mice: Quantitative Fluorescence Imaging and Analysis of Organs. Int J Nanomedicine. 2013; 8:1609–1620. [PubMed: 23637530]
34. Iyer AK, Khaled G, Fang J, Maeda H. Exploiting the Enhanced Permeability and Retention Effect for Tumor Targeting. Drug Discov Today. 2006; 11:812–818. [PubMed: 16935749]
35. Smith BR, Kempen P, Bouley D, Xu A, Liu Z, Melosh N, Dai H, Sinclair R, Gambhir SS. Shape Matters: Intravital Microscopy Reveals Surprising Geometrical Dependence for Nanoparticles in Tumor Models of Extravasation. Nano Lett. 2012; 12:3369–3377. [PubMed: 22650417]
36. Walkey CD, Olsen JB, Guo H, Emili A, Chan WC. Nanoparticle Size and Surface Chemistry Determine Serum Protein Adsorption and Macrophage Uptake. J Am Chem Soc. 2012; 134:2139–2147. [PubMed: 22191645]
37. Salvati A, Pitek AS, Monopoli MP, Prapainop K, Bombelli FB, Hristov DR, Kelly PM, Aberg C, Mahon E, Dawson KA. Transferrin-Functionalized Nanoparticles Lose Their Targeting Capabilities When a Biomolecule Corona Adsorbs on the Surface. Nat Nanotechnol. 2013; 8:137–143. [PubMed: 23334168]
38. Heldin CH, Rubin K, Pietras K, Ostman A. High Interstitial Fluid Pressure-an Obstacle in Cancer Therapy. Nat Rev Cancer. 2004; 4:806–813. [PubMed: 15510161]
39. Monopoli MP, Pitek AS, Lynch I, Dawson KA. Formation and Characterization of the Nanoparticle-Protein Corona. Methods Mol Biol. 2013; 1025:137–155. [PubMed: 23918335]

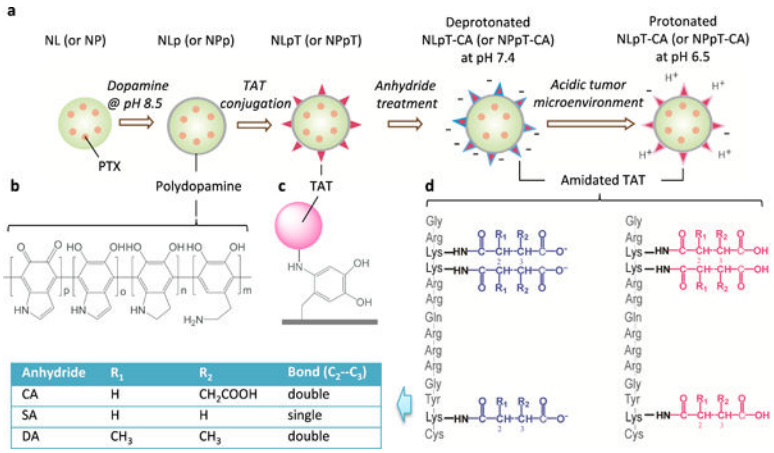

Fig. 1.

(a) Schematic description of nanoparticle preparation and their pH-sensitivity. NL: Bare lipid-shelled PLGA nanoparticles; NP: Bare PLGA nanoparticles; NLp: polydopamine (pD)-coated NL; NPp: pD-coated NP; NLpT: TAT-conjugated NLp; NPpT: TAT-conjugated NPp; NLpT-CA: cis-aconitic anhydride (CA)-treated NLpT; NPpT-CA: CA-treated NPpT. (b) Chemical structure of polydopamine (pD). Dopamine molecules are first oxidized and covalently linked to each other to form pD chains.[25] (c) TAT peptide conjugation to pD layer via a reaction between amine groups of TAT and quinone of pD. Adapted from ref.[23] (d) Chemical structures of amidated TAT at pH 7.4 and pH 6.5. Acid anhydrides preferentially react with the amine group of lysine residue to form β-carboxylic amide bond. The cationic guanidinyl group of arginine residue is not easily amidated.[24]

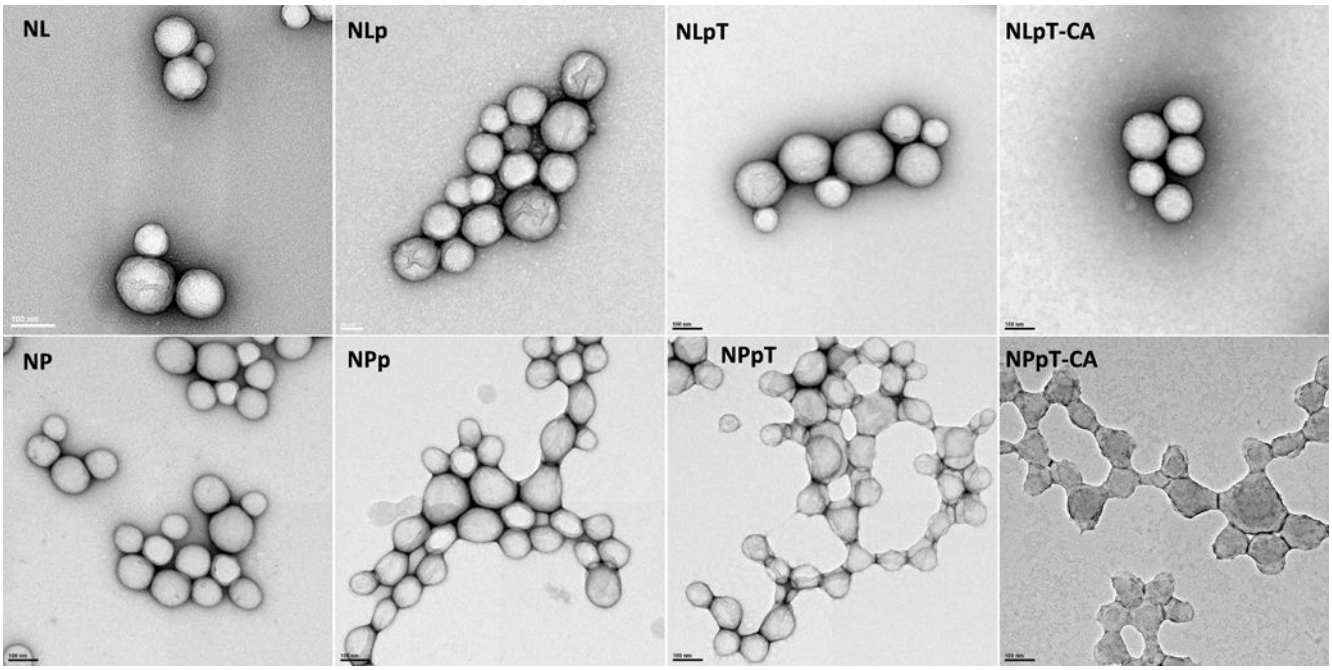

Fig. 2.

Transmission electron microscopic images of nanoparticles. NL: Bare lipid-shelled PLGA nanoparticles; NLp: pD-coated NL; NLpT: TAT-conjugated NLp; NLpT-CA: CA-treated NLpT; NP: Bare PLGA nanoparticles; NPp: pD-coated NP; NPpT: TAT-conjugated NPp; NPpT-CA: CA-treated NPpT. Particles were negatively stained with 1% uranyl acetate. Scale bars = 100 nm.

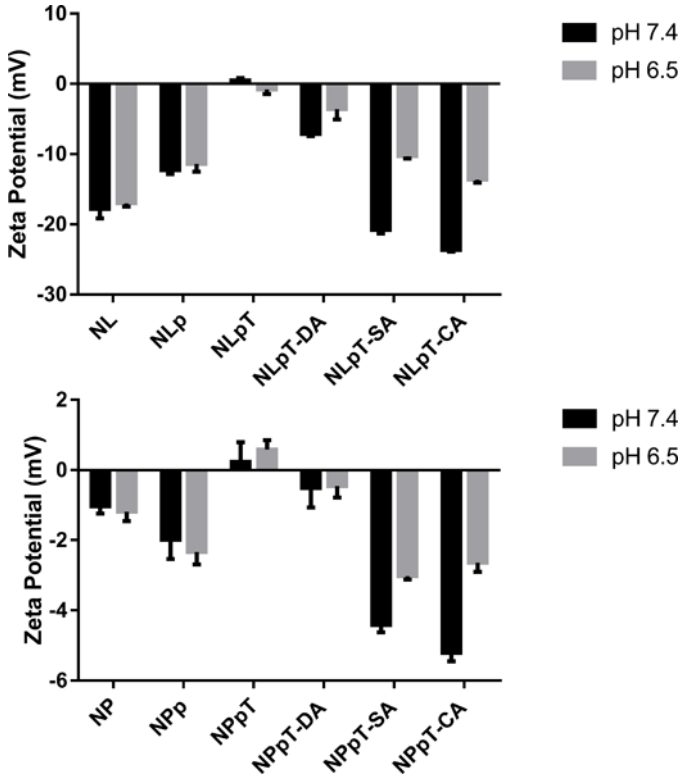

Fig. 3.

Zeta potential of nanoparticles at pH 7.4 and pH 6.5. NL: Bare lipid-shelled PLGA nanoparticles; NLp: pD-coated NL; NLpT: TAT-conjugated NLp; NLpT-DA: 2,3-dimethylmaleic anhydride (DA)-treated NLpT; NLpT-SA: Succinic anhydride (SA)-treated NLpT; NLpT-CA: CA-treated NLpT; NP: Bare PLGA nanoparticles; NPp: pD-coated NP; NPpT: TAT-conjugated NPp; NPpT-DA:DA-treated NPpT; NPpT-SA: SA-treated NPpT; NPpT-CA: CA-treated NPpT. n = 3 measurements of representative samples.

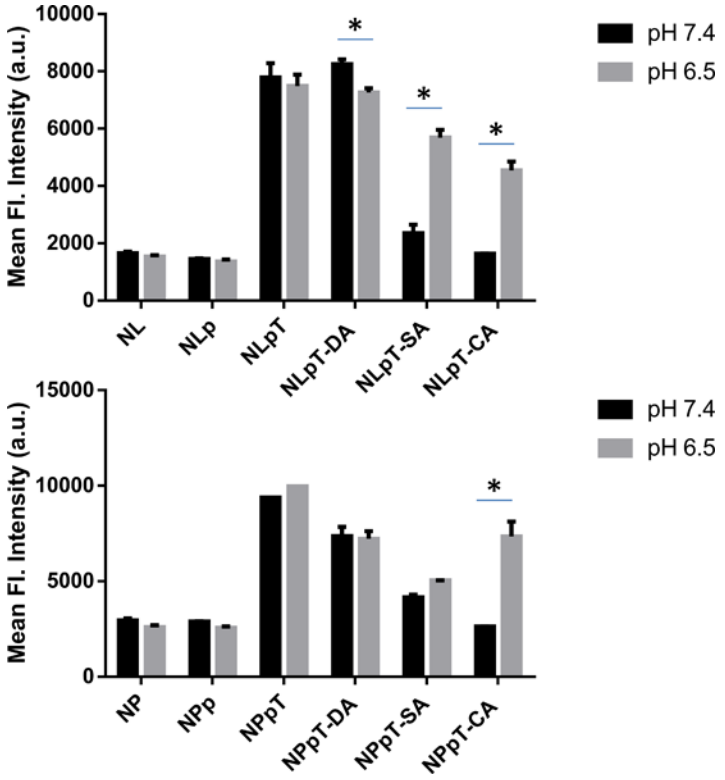

Fig. 4.

Cellular interactions of Rhodamine-labeled particles with LS174T cells in 2h incubation at pH 7.4 and pH 6.5, measured by flow cytometry. n = 2 or 3 identical and independent treatments. *: $p<0.01$ by Sidak's multiple comparisons test.

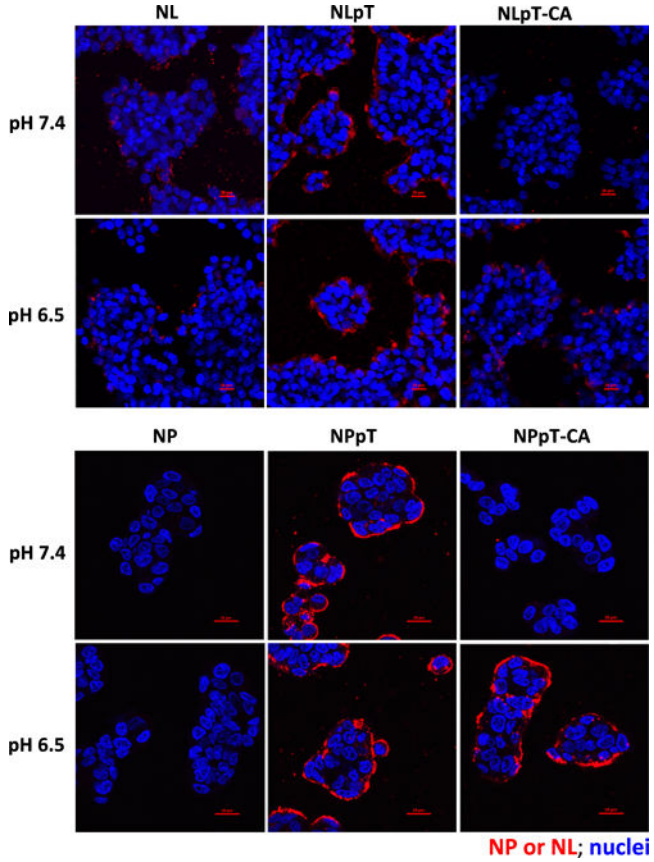

Fig. 5.

Confocal microscopic images of LS174T cells after treatment with Rhodamine-labeled particles for 2h. Red: Rhodamine-labeled particles; blue: Hoechst 33342-stained cell nuclei. Scale bars = 20 μm.

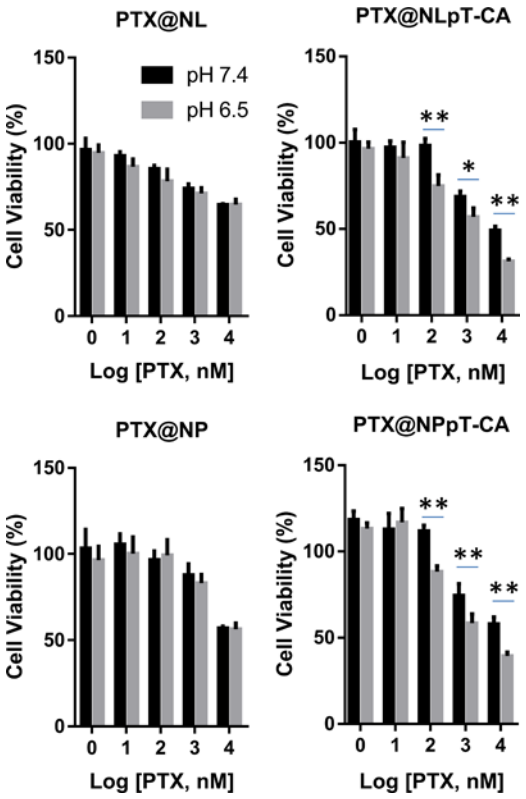

Fig. 6.

Cytotoxicity of PTX-loaded particles on LS174T cells at pH 7.4 and pH 6.5. n = 4 identical and independent treatments. *: $p<0.05$, **: $p<0.01$ by Sidak's multiple comparisons test.

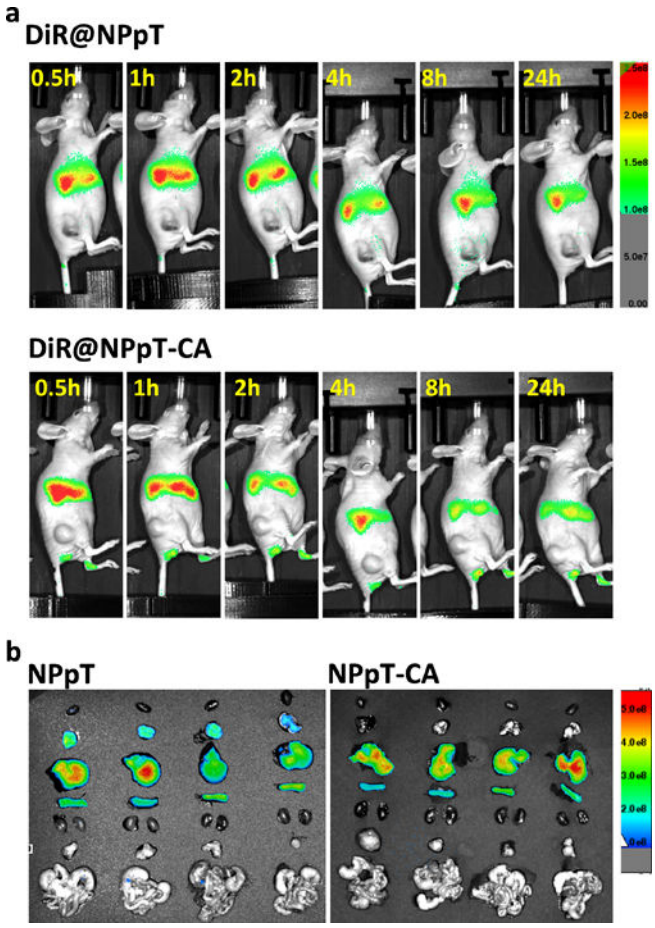

Fig. 7.

(a) Whole body imaging of a representative LS174T xenografted mouse that received DiR-loaded NPpT and NPpT-CA by intravenous injection. See Supporting Fig. 10 for all 4 animals per treatment. (b) Ex vivo imaging of major organs at 48 h post-injection. From the top: heart, lung, liver, spleen, kidneys, tumor, and gastrointestinal tract (n = 4 per treatment).

Table 1

Particle sizes measured by DLS

Nanoparticles	Description	Size (nm)	PDI[1]
NL	Bare lipid-shelled PLGA nanoparticles	230.1±4.57	0.106
NLp	pD-coated NL	258.6±6.37	0.139
NLpT	TAT-conjugated NLp	411.3±5.23	0.138
NLpT-CA	CA-treated NLpT	270.3±2.73	0.100
NLpT-SA	SA-treated NLpT	328.5±2.28	0.125
NLpT-DA	DA-treated NLpT	499.23±47.3	0.210
NP	Bare PLGA nanoparticles	163.1±1.70	0.073
NPp	pD-coated NP	165.9±3.82	0.115
NPpT	TAT-conjugated NPp	177.0±3.25	0.050
NPpT-CA	CA-treated NPpT	179.5±3.89	0.012
NPpT-SA	SA-treated NPpT	235.4±1.56	0.131
NPpT-DA	DA-treated NPpT	198.8±3.75	0.083

[1]Polydispersity index (PDI), an estimate of the width of the particle size distribution, obtained from the cumulant analysis as described in the International Standard on DLS ISO 13321:1996 and ISO 22412:2008 (Malvern DLS technical note MRK1764-01). PDI < 0.1 is considered monodisperse, and > 0.7 very broad.[28, 29]